MODEL TILT-ROTOR HOVER PERFORMANCE AND SURFACE PRESSURE MEASUREMENT

DTIC
ELECTE
JUN 0 4 1990
D

Chee Tung and Lonnie Branum

Research Scientists
U. S. Army Aeroflightdynamics Directorate, AVSCOM
NASA Ames Research Center
Moffett Field, California

AD-A222 535

ABSTRACT

A test of a small scale 3-bladed model rotor, with geometry typical of that used on tilt-rotor aircraft, was conducted in the Army Aeroflightdynamics Directorate's anechoic hover chamber. The purpose of this test was to determine the hover performance of the rotor and investigate the pressure distributions on a blade at various collective pitch angles and tip speeds. The measured pressures indicate that the rotor did not stall for high collective pitch angles up to $\theta_c = 25°$. This is clearly a three dimensional effect since two-dimensional theory predicts flow separation at these high angles. The flow near the trailing edge separated above $\theta_c = 25°$ which caused a sharp increase in power.

NOTATION

c	= rotor chord length, in
C_L	= blade section lift coefficient
C_P	= blade surface pressure coefficient
C_Q	= rotor torque coefficient
C_T	= rotor thrust coefficient
FM	= rotor figure of merit
r	= blade radial station, in
R	= rotor radius, 24 in
t/c	= maximum thickness to chord ratio
x	= chordwise distance from leading edge, in
β	= blade twist relative to 3/4 radius, deg.
θ_c	= collective pitch at 3/4 radius, deg.
σ	= rotor solidity, 0.1194

INTRODUCTION

The accurate prediction of hover performance is particularly important for tilt-rotors since the payload is about thirty percent of the aircraft's gross weight. NASA Ames Research Center has recently conducted a series of tests to measure the tilt-rotor hover performance and wake geometry at various test conditions

(Refs. 1,2). Reference 3 reported the correlation of these test results with predictions using a rotorcraft analysis program CAMRAD. They found that the theory underpredicts the ATB rotor hover figure of merit at high thrust coefficients (C_T/σ greater than 0.14). In addition, the measured figure of merit remains a constant value at high thrust coefficients where the prediction drops off. The authors further ruled out the possibility of wake geometry effects on hover performance by implementing the measured wake geometry into the CAMRAD code. They speculated that the airfoil stall model used in the CAMRAD code may be the major source of error. As reported in Ref.4, the CDI EHPIC free wake code shows good agreement between prediction and test results at moderate thrust coefficients for the XV-15 tilt-rotor. The under-prediction of figure of merit at high thrust suggests that the stall model that is implied in two-dimensional airfoil data may again be the source of error.

The present paper is aimed at clarifying the reason why these hover rotor codes failed to predict the tilt-rotor hover performance at high thrust levels. A small scale 3-bladed model rotor was tested in the Army Aeroflightdynamics Directorate's anechoic hover chamber. The blade was instrumented with surface pressure taps. Hover performance and selected surface pressures were recorded. Finally, a finite-difference code FPR coupled with CDI's free wake code has been used to predict surface pressures.

DESCRIPTION

Rotor

The rotor tested is a 3-bladed rotor designed to operate at thrust coefficients typical of current tilt-rotor aircraft, such as the XV-15 tilt-rotor, but is not actually scaled to any particular full scale configuration. The rotor was mounted on the Aeroflightdynamics Directorate's rotary wing test stand in the Army hover

chamber as shown in Fig. 1. The rotor system has a diameter of 4 feet and a solidity of 0.1194. The blades are constructed out of birch wood and have a total twist of 32° between the root cutout and the tip. Table 1 gives the twist, chord, and maximum thickness distributions of the blade with the radius. The blade section airfoils were originally designed to represent NACA 64 series airfoils however, templates made of 12 radial locations along the blade showed that the actual airfoil sections differed from that series. These templates were digitized so that the actual airfoil geometry could be used in the prediction codes. The actual airfoil coordinates will be included in a NASA Technical Memorandum containing the test data. To obtain pressure data for this test, one of the blades was configured with a total of nineteen 0.03 inch diameter pressure tubes. Ten of these tubes were embedded radially along the upper surface of the blade while the remaining tubes were embedded radially along the lower surface. Tap orifices were located at eight radial locations on each pressure tube. Table 2 shows the tap location for both the chordwise and radial directions. Fig. 2 shows a partial view of the pressure orifices on the upper surface of the blade.

Instrumentation

Each one of the nineteen pressure tubes in the blade was connected to a corresponding Kulite (YQC-250 series) differential pressure transducer using flexible plastic tubing. These pressure transducers were located inside a container above the rotor hub (Fig. 2). As shown in the figure the transducers were set close to the center of rotation and aligned vertically so that centrifugal force would not affect the transducer. Calibration checks of each transducer were performed on a daily basis prior to running. A six component strain gauge balance was used to measure thrust and torque data from the rotor. Other measurements included ambient temperature and pressure and rotor rpm. Rotor rpm was measured using a 60/rev counter. All data were recorded using an HP data acquisition system. Thrust, torque and blade pressure data were averaged over 22 rotor revolutions.

Test conditions and procedures

Performance and pressure data were obtained at collective pitch angles ranging from 0° to 28° and rotor speeds of 400, 600, 800, 1200, 1800, and 2400 rpm. This paper discusses the 1800 rpm rotor speed case primarily. The collective pitch angles were manually set at the hub for each blade using a template at the 3/4 radius and a digital protractor. Pressure data were collected at one radial location at a time since each tube had eight tap orifices per transducer. This was accomplished by sealing off seven radial locations and

leaving the one remaining radial location open for data measurement. Once data were obtained for that particular collective and radial location another radial location was opened and the previous one sealed off. This was done until data at all eight radial locations were recorded. The collective was then changed and the process was repeated.

TEST RESULTS

Hover Performance Data

Although the test matrix consists of many test points, only limited data are presented here. The complete data will be included in a NASA TM to be published. The data at 1800 rpm are reported in detail. Other data are similarly consistent. The tip speed equal to 377 feet per second at 1800 rpm corresponds to approximately six-tenths of full-scale tip speed. The tip Reynolds number is about 750,000. Fig.3 shows the effect of collective pitch angle on C_T/σ. The solid line represents the two different rates of increasing C_T/σ with respect to collective pitch angles. The C_Q/σ as a function of collective pitch angle is given in Fig.4. The solid line in this figure represents a third-order polynomial least-squares curve fit of the data. The C_Q/σ versus $(C_T/\sigma)^{1.5}$ is shown in Fig.5. A linear relation is observed for $(C_T/\sigma)^{1.5}$ up to 0.087. The figure of merit for this rotor is shown in Fig.6 as a function of C_T/σ. The figure of merit reaches a plateau at 0.75 between C_T/σ equal to 0.1 and 0.17 and drops off quickly afterward.

Pressure Coefficients

The column of air inside the pressure tube is subjected to centrifugal force, so the measured pressure coefficients need to be corrected for this effect. This correction was completed during data reduction. The flexible tubing between the pressure tube at the 85 percent chord location on the upper surface of the blade and its transducer was not functional during the early part of the test but was repaired later in the test. Because of this some of the figures do not contain pressure information for that location. In addition, pressure data from the 60 percent chord location on the lower surface of the blade was not obtained due to an inoperable transducer. Typical sectional pressure distributions are shown in Fig.7 for $\theta_c = 8°$ and 1800 rpm. Figs.8 and 9 are the plots of C_P distributions over a range of collective angles at r/R=0.2 and r/R=0.75 respectively. The surface pressure distributions over a range of rotor speeds are shown in Figs. 10 and 11 respectively. From observation the C_P does not change very much with the

rotor speed and the 1800 rpm results are representative of all measurements obtained.

Sectional Lift Coefficients

Accurate calculation of sectional lift coefficients from pressure distributions requires many pressure measurements located near the leading edge. The present study has only one pressure measurement at six percent chord on the upper surface and one at ten percent chord on the lower surface of the blade. Therefore, an approximate method (Ref.5) to estimate the pressure coefficients near the leading edge was employed. This method approximates the actual airfoil by using a simpler airfoil with an elliptical nose. The exact solution for the approximating airfoil leads to simple expressions which are accurate at the nose of the actual airfoil. When this method applies to the rotor problem, the exact solution for the approximating airfoil contains two unknown constants namely the sine and cosine of the local inflow angle. The measured pressures at six percent chord on the upper surface of the blade and the one at ten percent chord on the lower surface of the blade were used to determine these two unknowns. Fig. 12 shows the sectional lift coefficients as a function of collective pitch angle at 1800 rpm. The lift coefficients at $\theta_c = 12°$ are omitted here due to some erroneous pressure measurements.

DISCUSSION AND CORRELATION

The chordwise pressure distributions show no sign of flow separation near the leading edge on the upper surface of the blade. This is true even for the very high thrust conditions shown in Fig.8. No loss of leading edge pressure on the blade implies no loss of lift at that radial station and no drop in total thrust. This may explain why the thrust of the rotor does not decrease at high collective pitch angles. Further analysis of the surface pressures show that the flow does separate near the trailing edge at the higher collective pitch angles ($\theta_c > 25°$) in Fig.9. Fig.13 shows the surface pressure coefficients at the three rearmost upper pressure taps at $r/R = .75$ and various thrust conditions. The sharp change in C_P first occurs for $x/c = .95$ around $(C_T/\sigma)^{1.5} = .075$ and the C_P at $x/c = .85$ increases around $(C_T/\sigma)^{1.5} = .085$. It seems that the trailing edge separation moves forward toward the leading edge as C_T increases. The inboard section behaves in a similar manner. The trailing edge separation increases the drag force at that section and so increases the total power. Thus the total power increases sharply at higher collective pitch angles as seen in Fig.4. It was observed that the flow does separate around mid-chord at radial

station $r/R = .125$. It is suspected that the flow separates at the root cutout and spills over the pressure taps.

Himmelskamp in reference 6 conducted measurements of pressure distributions on a rotating propeller and determined local lift coefficients of the blade. He found that a marked increase in lift coefficient occurred near the hub at high angles of incidence. He suggested that the Coriolis force, which occurs in the rotating system of reference, acts as a favorable chordwise pressure gradient to delay flow separation and that the influence of centrifugal force is to reduce the boundary layer thickness. These are the two major reasons why higher lift is generated.

The CDI's EHPIC code and AMI's HOVER code (Refs.7 and 8) coupled with the FPR code (Ref.9) were used to compute the surface pressure distributions. The first two codes are based on an integral method where the rotor blades and wakes are represented by vortex segments. The FPR code is a finite difference scheme for solving the full-potential equation. The EHPIC and HOVER codes were not used for stand-alone calculations of performance because no two-dimensional airfoil data are available. In essence the FPR solution was used to replace the airfoil section tables. The technique to couple the finite difference code with the integral code has been reported in Ref. (10) . A set of partial inflow angles are generated by using either the EHPIC or HOVER codes and these angles are passed to the FPR code. The partial inflow angle is defined as the inflow angle due to partial wakes excluding the near wake inside the finite difference grid. As mentioned in the previous section, the actual sectional airfoils are not quite the same as the NACA 64 series airfoil sections. The digitised coordinates of the experimental blade do not have the smoothness (continuous slope and curvature) of the actual airfoils. The unevenness of the predicted pressure distributions is a consequence of these discontinuities. Fig.14 shows the comparison of predicted pressure distributions with measurements at $\theta_c = 16°$ and 1800 rpm. Good agreement is seen at outboard radial sections while the EHPIC/FPR code overpredicts the lift at the inboard sections. This means that the EHPIC code overpredicts the partial inflow angles at inboard sections. The last inboard grid for the FPR code is at r/R=0.135, thus the predicted surface pressures at that section are used to compare the measurements at r/R=0.125. The AMI's HOVER code gives about the same partial inflow angles as the EHPIC code if the same wake geometry is used. Similar pressure results are obtained. The EHPIC code fails to converge at $\theta_c = 28°$, so a set of partial inflow angles by HOVER code using a prescribed wake geometry and modified inboard partial inflow angles are used to get

a better comparison as shown in Fig.15. But the FPR prediction does not match the pressure data near the trailing edge stations where the flow separates.

The present experiment points out that the predicted inflow angles generated by the lifting-surface codes at the inboard sections are not correct. The experimental Reynolds number was 100,000 to 1,000,000 which is much less than full-scale. This may have been a significant factor in the overpredicted inflow angles. The overprediction of these inflow angles gives higher viscous drag than the two-dimensional airfoil tables and lowers the figure of merit. It is suspected that the same situation may happen to the full-scale rotor. One may also speculate that a new rotor with inboard airfoil sections that delay the trailing edge separation will improve the rotor hover performance. The ATB rotor tested in Ref.3 has a constant blade thickness ratio from r/R=.3 to r/R=.75 which is far less then the one used on the XV-15 rotor. Usually, the thicker airfoil stalls early from the trailing edge. The ATB blade has better hover performance at high thrust coefficients which may be due to the delay of trailing edge separation. More investigations are needed to verify this hypothesis.

CONCLUSIONS

A large number of surface pressure data and hover performance information from a model tilt-rotor was collected and analysed. Some important conclusions that can be drawn from this study are:

1) The model rotor does not show flow separation near the leading edge on the upper surface of the blade at the various rotational speeds and collective pitch angles that were tested. This means that measurements show no reduction in thrust even at very high collective pitch angles.

2) The flow separates near the trailing edge at collective pitch angles greater than 25° which in turn causes a sharp increase in power.

3) Hover free wake codes like EHPIC and HOVER coupled with FPR code can predict the surface pressure well for collective pitch angles less than 22° on the outboard sections only (r/R > 0.5). However, both codes overpredict the inboard partial inflow angles.

4) For the Reynolds number range of 100,000 to 1,000,000 it is clear that any analytical performance model must accurately predict the effects of separated flow.

REFERENCES

[1]Felker, F. F., Young, L. A. and Signor, D. B., "Performance and Loads Data From a Hover Test of a Full-Scale Advanced Technology XV-15 Rotor," NASA TM-86854, January 1986.

[2]Felker, F. F., Young, L. A., Signor, D. B. and Betzina, M. D., "Performance and Loads Data From a Hover Test of a 0.658-Scale V-22 Rotor and Wing," NASA TM-89419, April 1987.

[3]Felker, F. F., Maisel, M. D. and Betzina, M. D., "Full Scale Tilt Rotor Hover Performance," *Journal of the American Helicopter Society*, Vol. 31, No. 2, April 1986.

[4]Quackenbush, T. R., Bliss, D. B., Wachspress, D. A. and Ong, C. C., "Free Wake Analysis of Hover Performance Using a New Influence Coefficient Method," C. D. I. Report No. 87-03, July 1987.

[5]Roshko, A. "Pressure distribution at the Nose of a Thin Lifting Airfoil," Douglas Aircraft Company Report No. SM-23368, November 1958.

[6]Himmelskamp, H., "Profile Investigations on a Rotating Airscrew," Reports and Translations No. 832, September 1947.

[7]Bliss, D. B., Wachspress, D. A., Quackenbush, T. R. and Bilanin, A. J., "A New Approach to the Free Wake Problem for Hovering Rotors," C. D. I. Report No. 84-07, June 1984.

[8]Summa, J. M. and Clark, D. R., "A Lifting-Surface Method for Hover/Climb Loads," *Presented at the 35th Annual National Forum of the American Helicopter Society*, Reprint No.79-1, May 1979.

[9]Strawn, R. C. and Caradonna, F. X., "Numerical Modeling of Rotor Flows with a Conservative Form of Full-Potential Equations," AIAA Paper 86-0079, January 1985.

[10]Caradonna, F. X., Desopper, A. and Tung, C., "Finite Difference Modeling of Rotor Flows Including Wake Effects," *Presented at the 8th European Rotorcraft Forum*, August 1982.
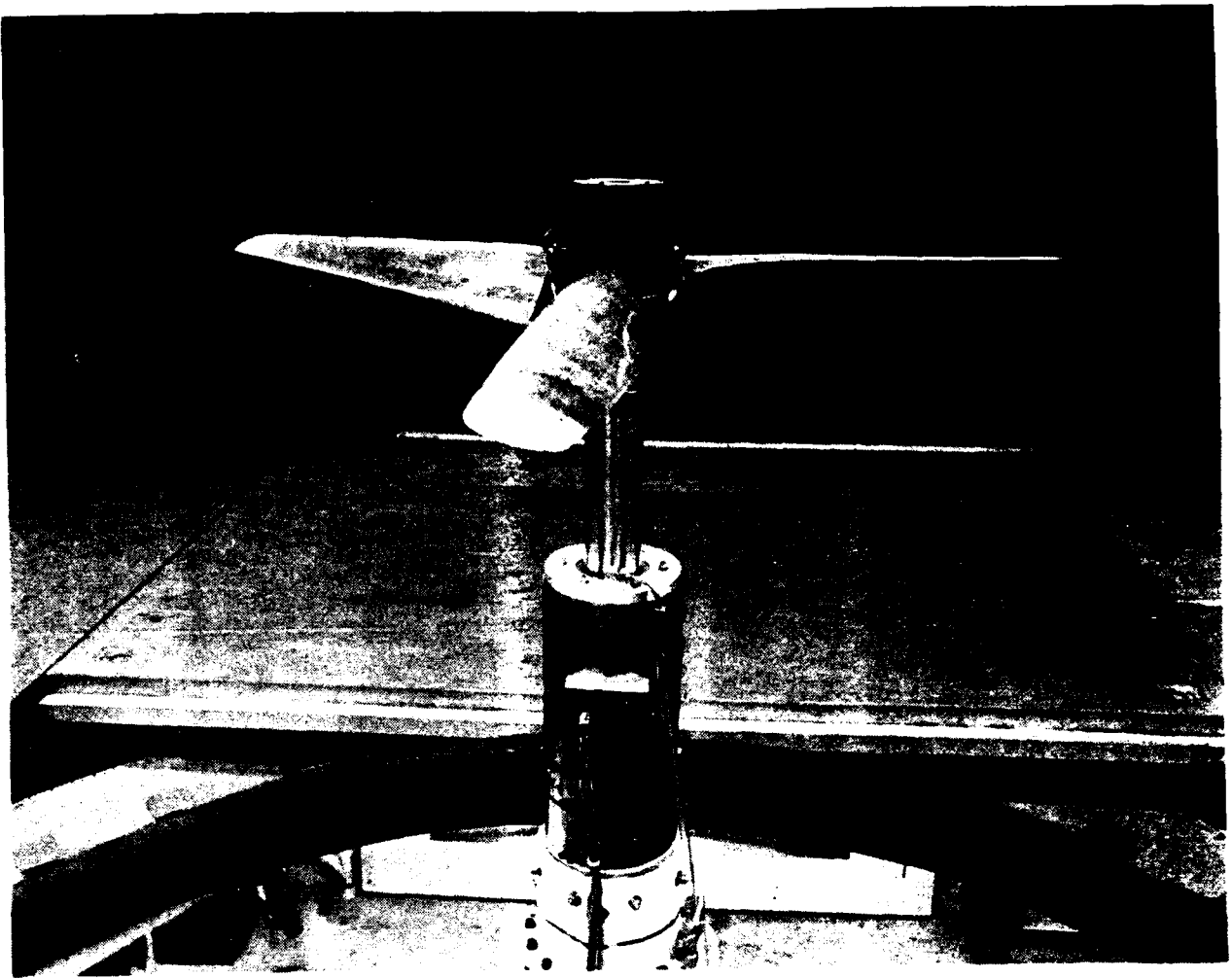
Figure 1. Three-bladed model rotor in the Army Anechoic Hover Chamber.

Table 1. Blade characteristics.

r/R	β, deg	c, in	t/c
.125	26.7	4.06	.466
.20	23.2	4.06	.407
.30	17.8	4.02	.335
.40	11.1	3.89	.269
.50	8.2	3.75	.211
.60	3.8	3.58	.191
.70	2.2	3.38	.162
.75	0.0	3.23	.147
.81	-0.8	3.08	.138
.86	-2.6	2.92	.125
.91	-3.9	2.77	.120
.96	-4.6	2.52	.107

STATEMENT "A" per D. Kiefer
Army Aeroflightdynamics Directorate/FAZRT
AF-F, NASA Ames Research Center, Moffett
Field, CA 94035
TELECON   5/31/90   VG

Figure 2. Top view of the model rotor showing the pressure transducers and a partial view of the pressure blade.

Table 2. Tap locations for the (U)upper and (L)lower surface of the pressure blade.

%c / %R	6	10	15	25	30	35	40	45	50	55	60	65	70	75	80	85	90	95
12.5	U	L	U,L	U	L	U	L	U	L	U	L	U	L	U	L	U	L	U
20.0	U	L	U,L	U	L	U	L	U	L	U	L	U	L	U	L	U	L	U
30.0	U	L	U,L	U	L	U	L	U	L	U	L	U	L	U	L	U	L	U
40.0	U	L	U,L	U	L	U	L	U	L	U	L	U	L	U	L	U	L	U
50.0	U	L	U,L	U	L	U	L	U	L	U	L	U	L	U	L	U	L	U
60.0	U	L	U,L	U	L	U	L	U	L	U	L	U	L	U	L	U	L	U
70.0	U	L	U,L	U	L	U	L	U	L	U	L	U	L	U	L	U	L	U
75.0	U	L	U,L	U	L	U	L	U	L	U	L	U	L	U	L	U	L	U
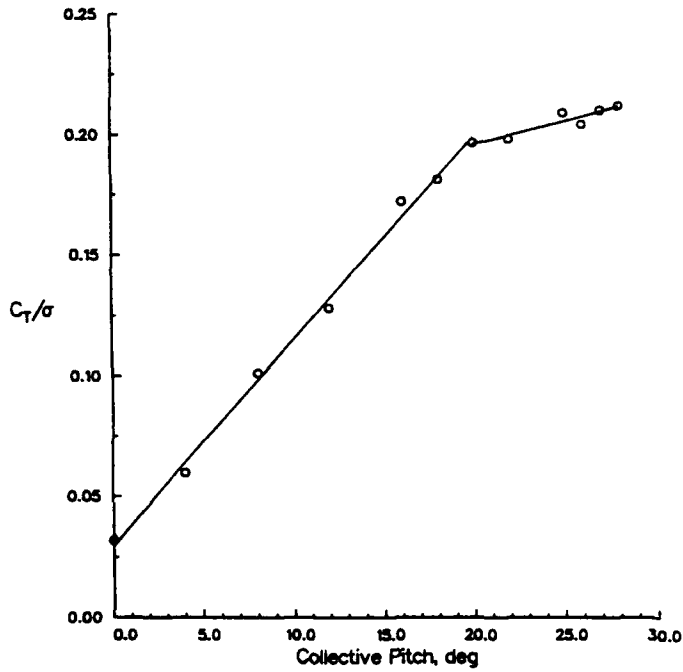
Figure 3. Effect of collective pitch on C_T/σ at 1800 rpm.
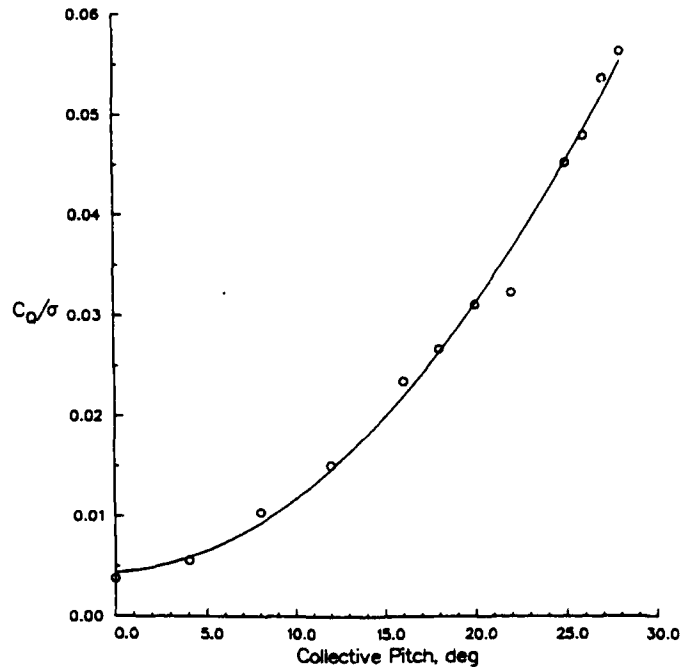
Figure 4. Effect of collective pitch on C_Q/σ at 1800 rpm.
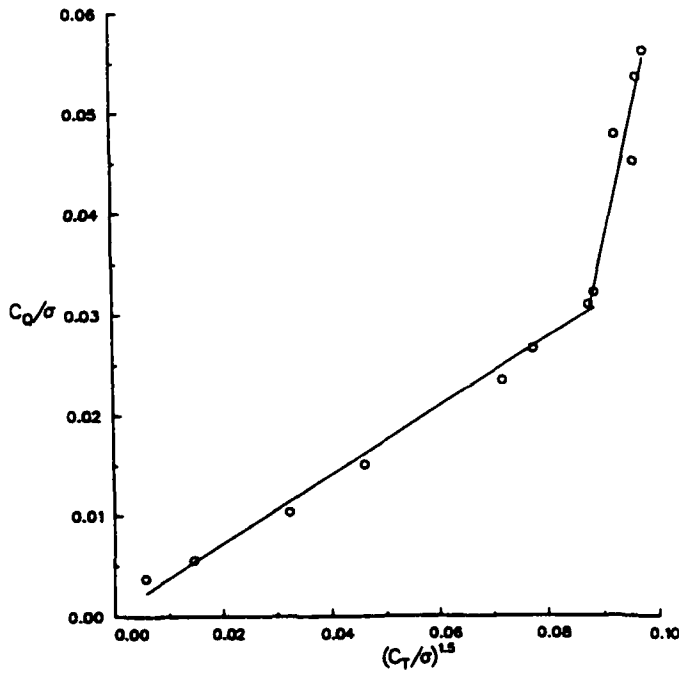
Figure 5. C_Q/σ as a function of $(C_T/\sigma)^{1.5}$ at 1800 rpm.
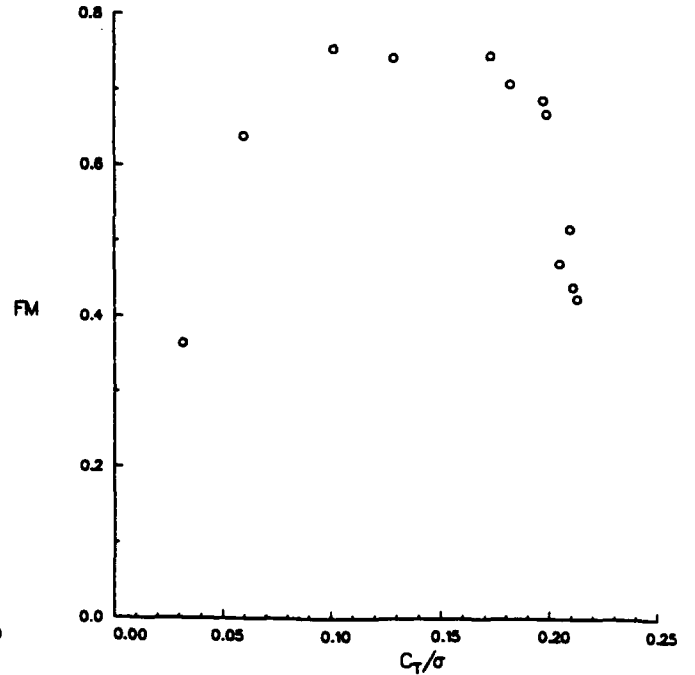
Figure 6. Effect of C_T/σ on rotor performance at 1800 rpm.
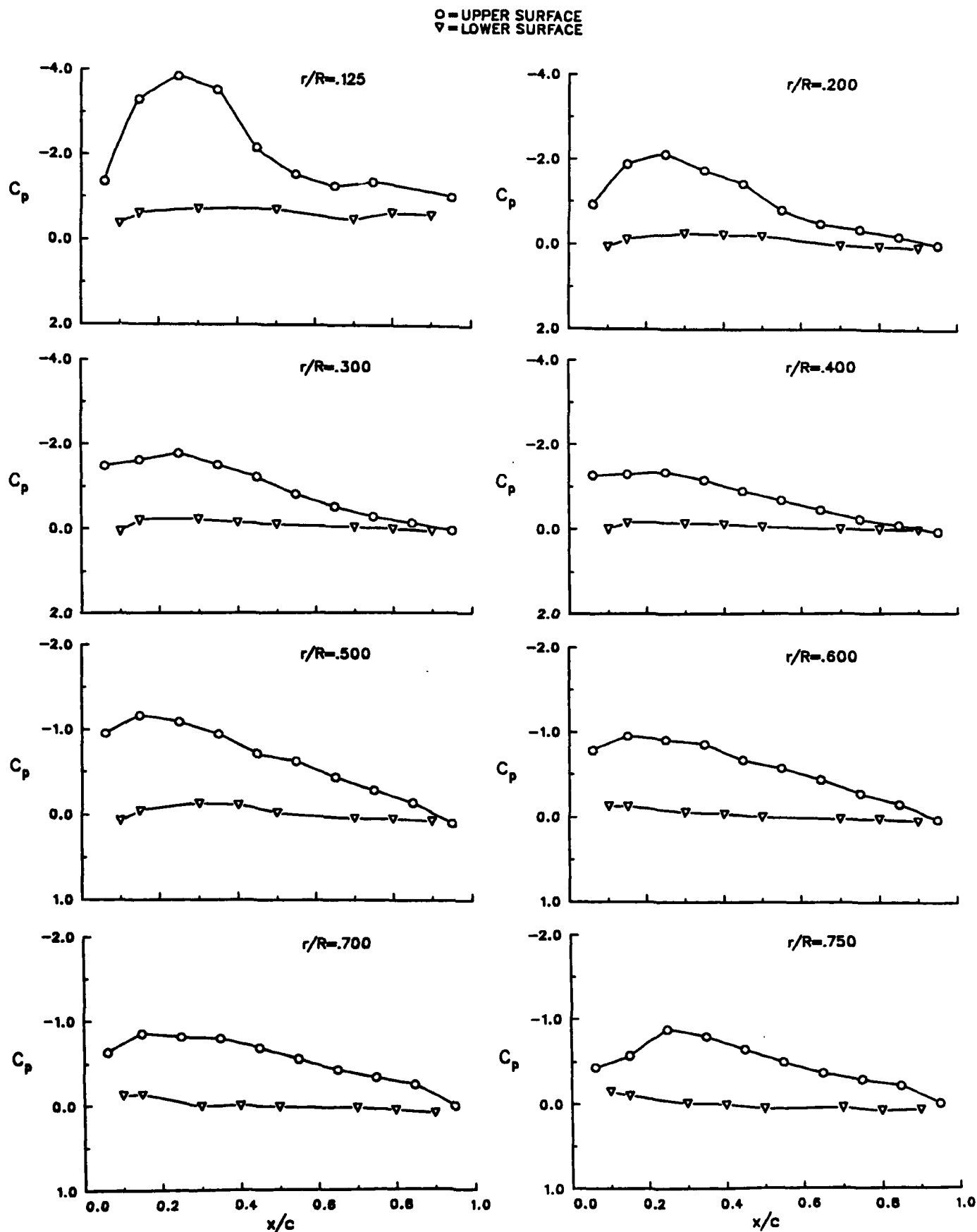
Figure 7. Chordwise pressure distributions along the blade radius. $\theta_c = 8°$, rpm=1800.

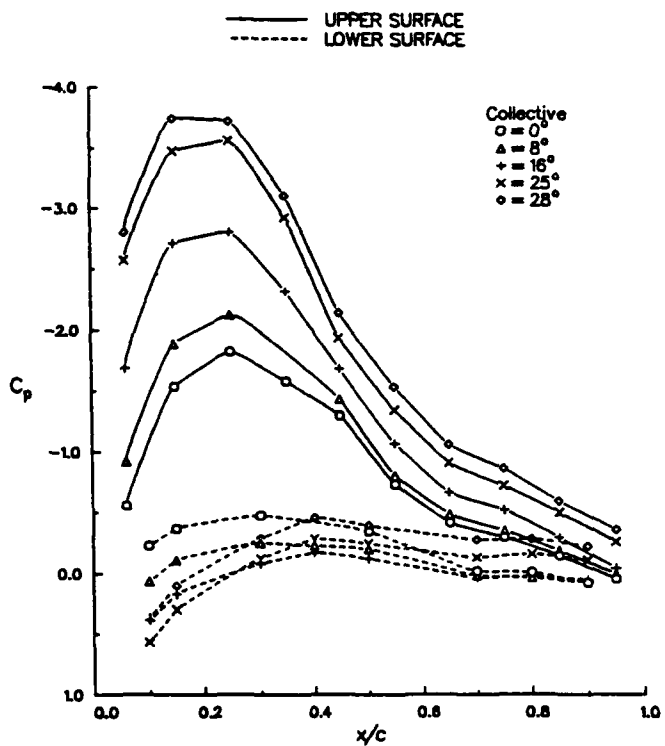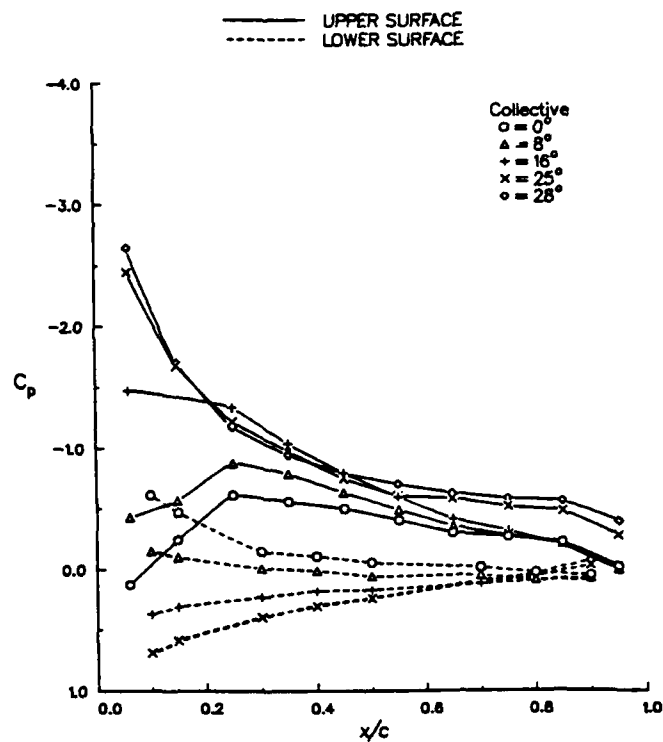Figure 8. Surface pressure distributions for a range of collective pitch angles. r/R=.20, rpm=1800.

Figure 9. Surface pressure distributions for a range of collective pitch angles. r/R=.75, rpm=1800.
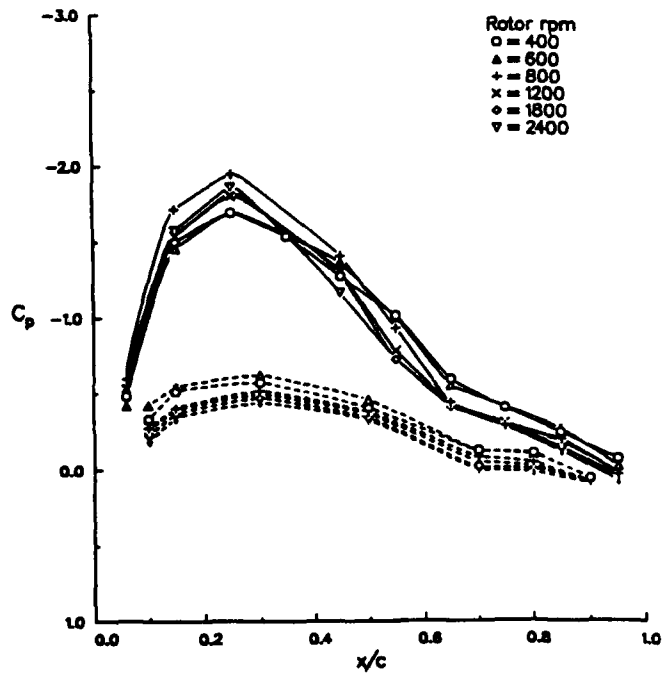
Figure 10. Surface pressure distributions for a range of rotor speeds. r/R=.20, $\theta_c = 0°$.
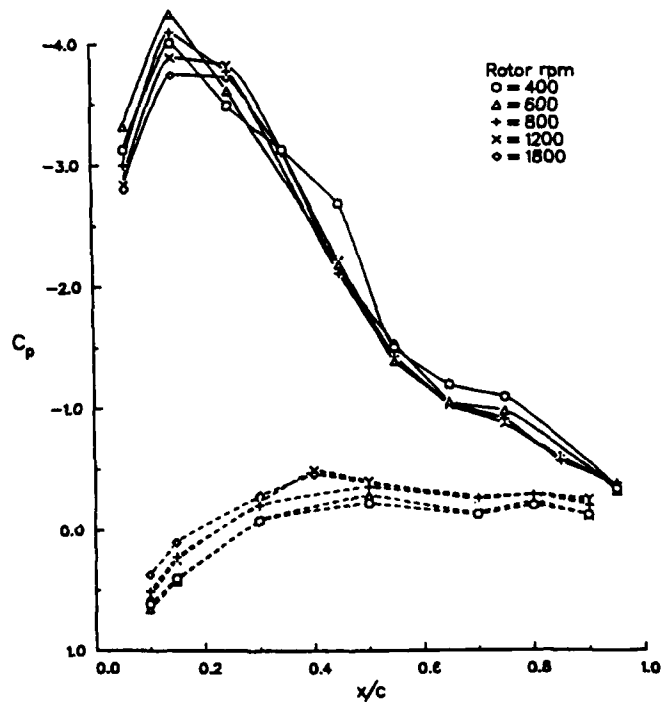
Figure 11. Surface pressure distributions for a range of rotor speeds. r/R=.20, $\theta_c = 28°$.
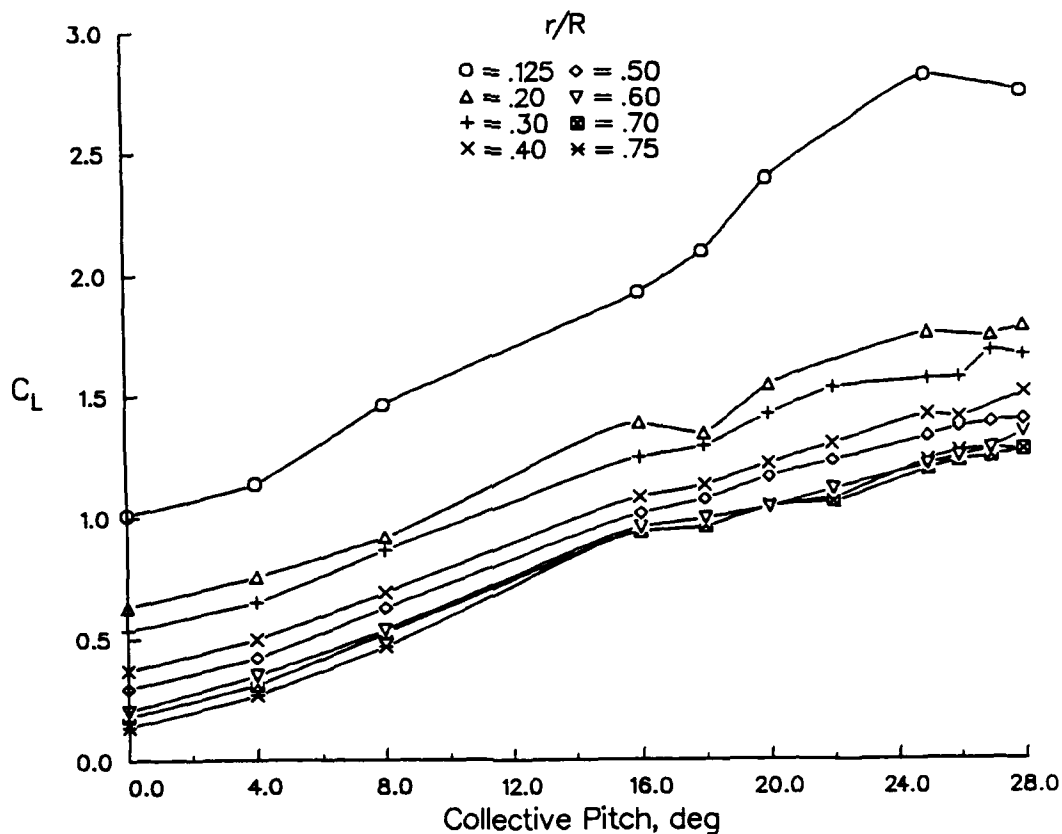
Figure 12. Blade sectional lift coefficients as a function of collective pitch at 1800 rpm.

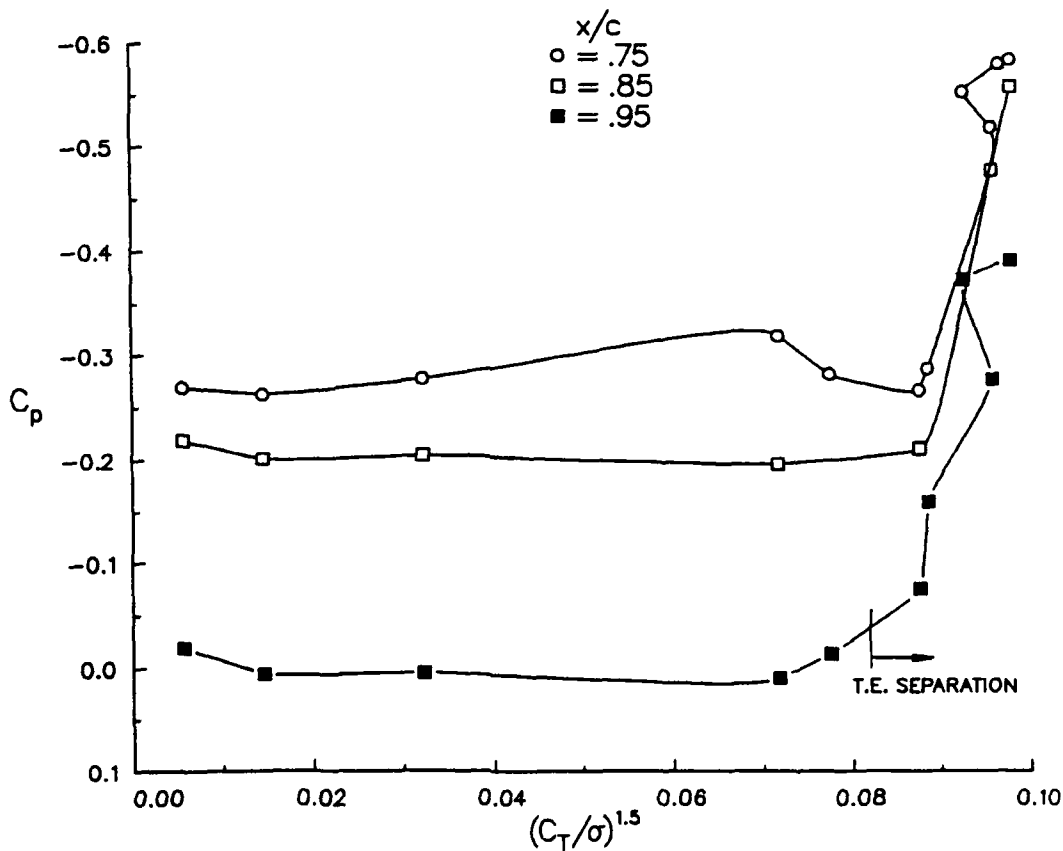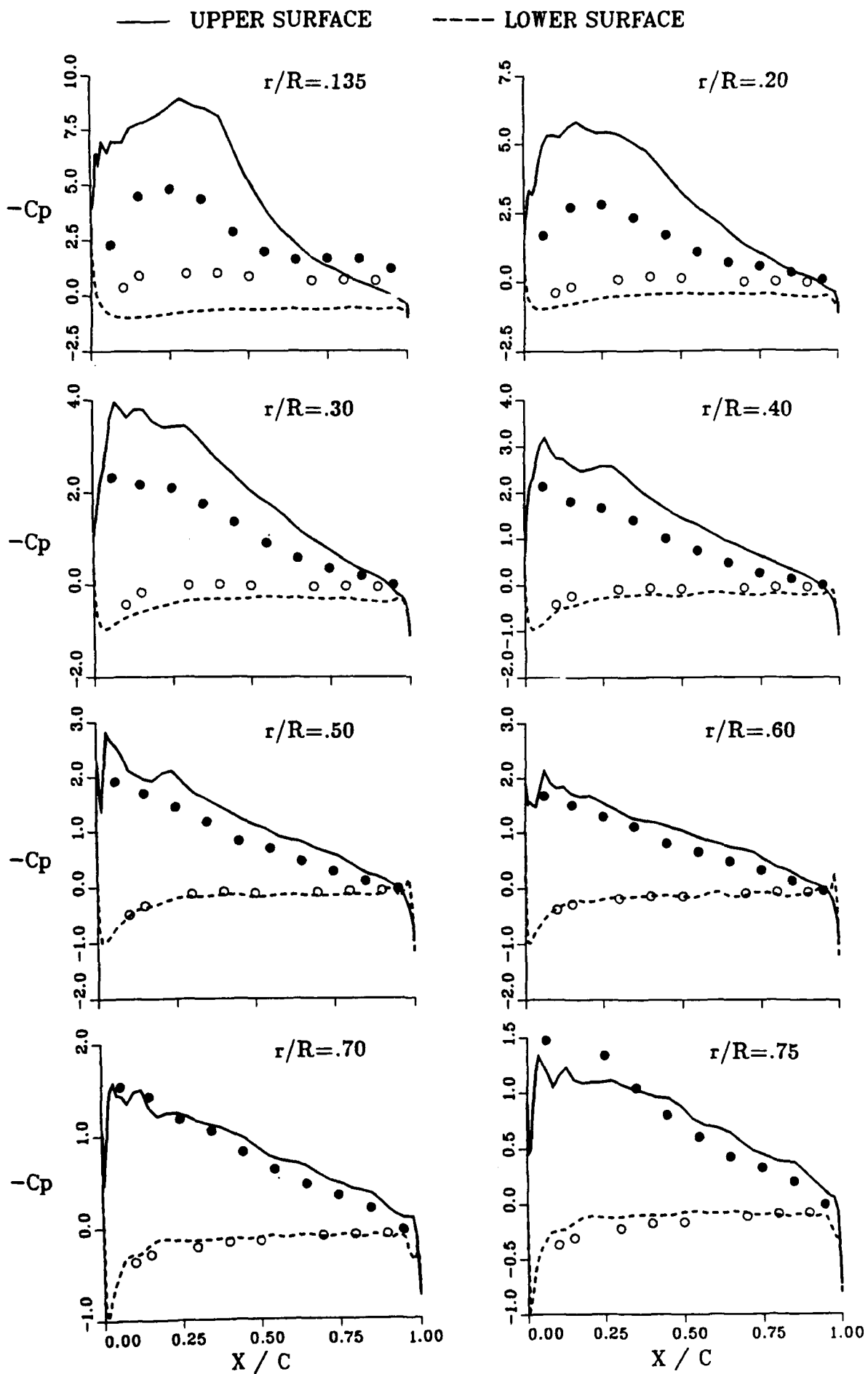Figure 13. Effect of increasing thrust on the three rearmost upper surface pressure taps. r/R=.75, rpm=1800.

Figure 14. Surface pressure results using predicted partial inflow angles by EHPIC code. $\theta_c = 16°$, rpm=1800. (Note: Raggedness in C_P result is due to unevenly digitized airfoil coordinates.)
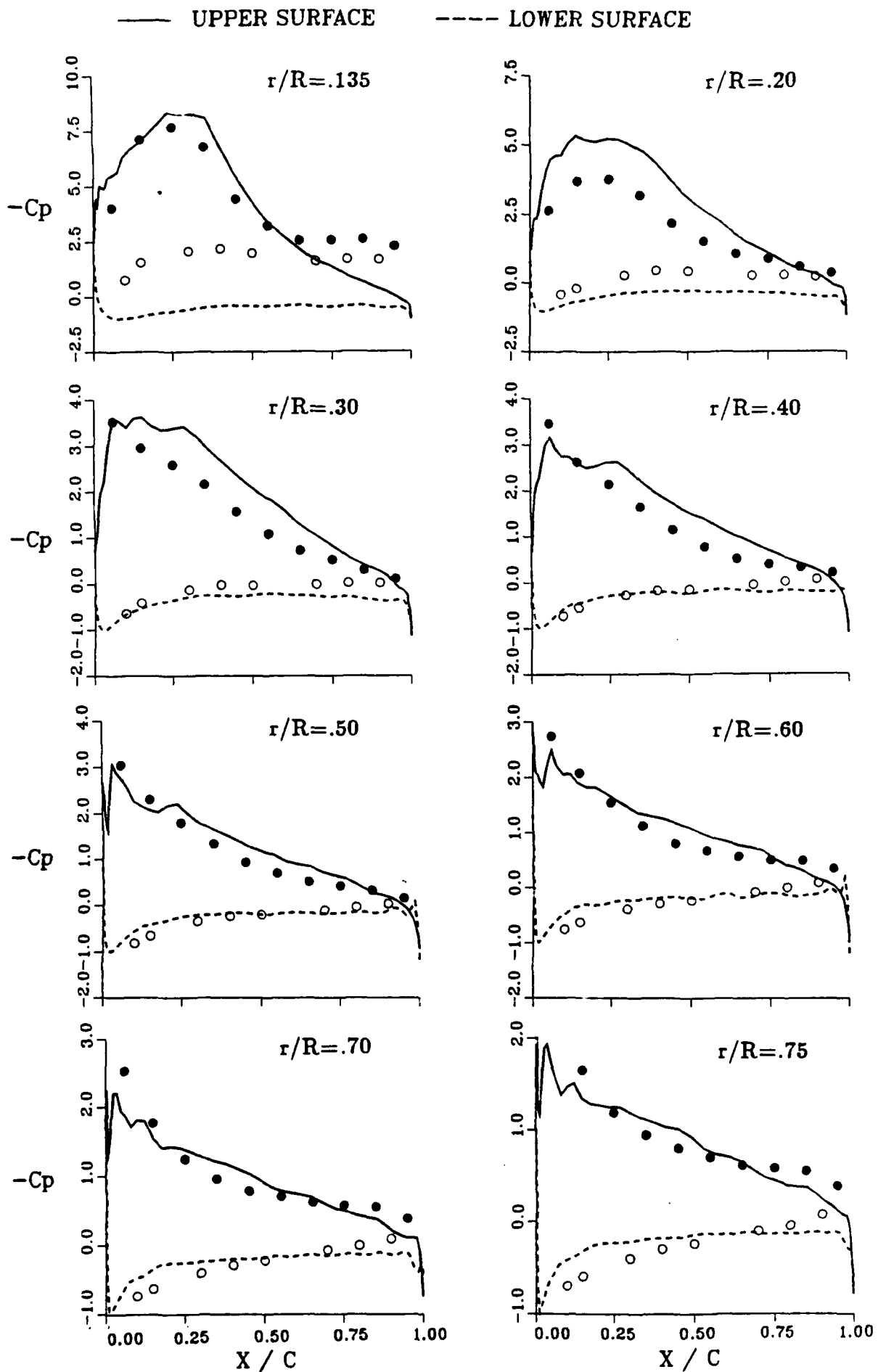
Figure 15. Surface pressure results using predicted partial inflow angles by HOVER code. $\theta_c = 28°$, rpm=1800. (Note: Raggedness in C_P result is due to unevenly digitized airfoil coordinates.)